Sedimentary rock porosity studied by electromagnetic techniques: nuclear magnetic resonance and dielectric permittivity

M. E. Ramia & C. A. Martín

Applied Physics A
Materials Science & Processing

ISSN 0947-8396

Appl. Phys. A
DOI 10.1007/s00339-014-8798-0

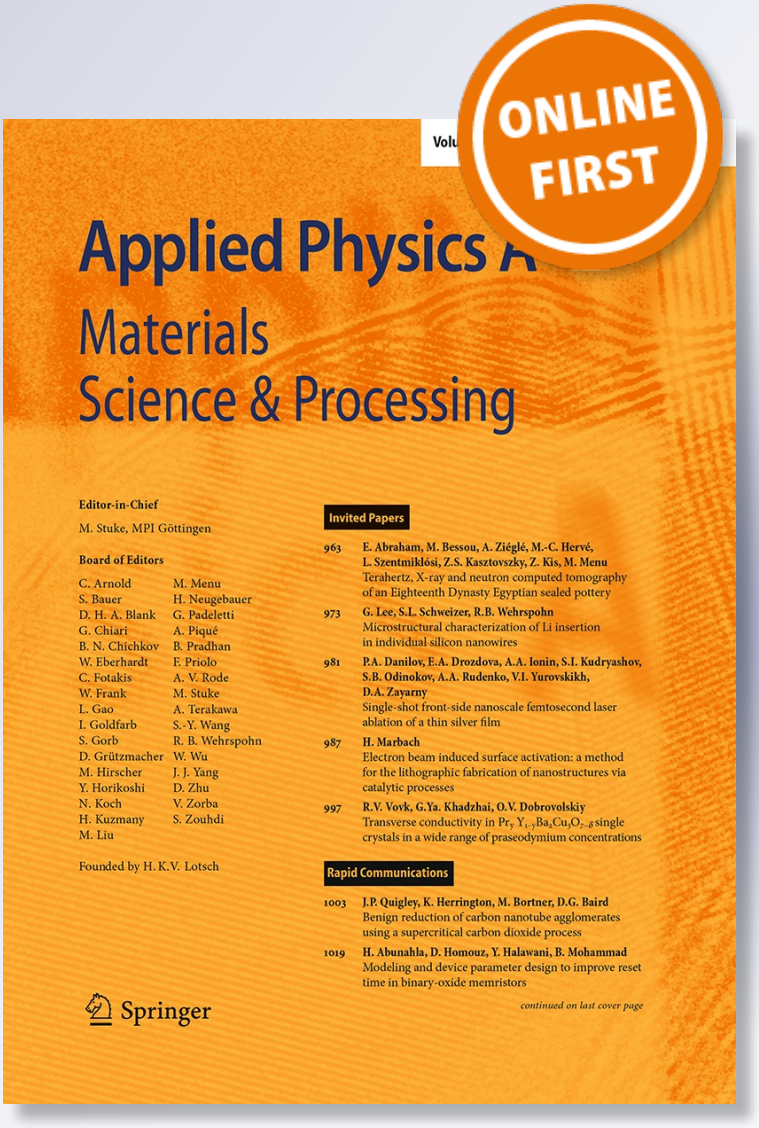

Springer

Appl. Phys. A
DOI 10.1007/s00339-014-8798-0

Applied Physics A
Materials Science & Processing

Sedimentary rock porosity studied by electromagnetic techniques: nuclear magnetic resonance and dielectric permittivity

M. E. Ramia · C. A. Martín

Received: 16 September 2013 / Accepted: 19 September 2014

Abstract The present work involves a comprehensive experimental study of porosity and pore size distribution of sedimentary rocks, from oil fields formations, by means of two electromagnetic techniques, namely proton (^{1}H) nuclear magnetic resonance (NMR) and dielectric complex constant (DCC) as function of the frequency, both providing complementary results. The NMR yields an accurate determination of the relative pore size distribution and both movable and irreducible fluids. The DCC measurement provides the direct current electrical resistivity of the samples with different degrees of hydration. Thus, combining the results of both techniques allows the determination of the tortuosity index, by means of Archie's relation, and from it the average pore channel length. These measurements are performed on fully hydrated (saturated), centrifuged, dried, and cleaned rocks and also on samples with the irreducible fluids. Finally, the results are complemented with capillary pressure measurements to obtain the total volume associated with the pore channels related to the rock permeability. Additionally, the work presents a particular method to use a network analyzer to measure the DCC.

1 Introduction

Experimental electromagnetic techniques such as the nuclear magnetic resonance (NMR) and the dielectric complex constant (DCC) have become nowadays valuable tools to study porous systems and wettability phenomena related to different materials. Both techniques are widely used although few cases are reported as complementary tools. Nevertheless, both the NMR and the DCC provide information from different scales namely from nearest-neighbors interactions to bulk responses, respectively. The NMR arises from the local interaction of the proton magnetic moments with a magnetic field, composed by a constant external magnetic field plus a local field from neighboring magnetic dipoles and paramagnetic impurities. On the other hand, the DCC is sensitive to polarization and ionic current in the sample, and to obtain DCC data, the displacement current through a capacitor filled with the rock under study is used. Additionally, an experimental method involving the use of a network analyzer to measure the DCC and its experimental limitations is presented.

M. E. Ramia (✉) · C. A. Martín
Facultad de Matemática Astronomía y Física, Universidad Nacional de Córdoba, 5000 Córdoba, Argentina
e-mail: ramia@famaf.unc.edu.ar

2 Experimental techniques

2.1 The NMR

In a fully hydrated pore, the most relevant relaxation mechanisms of a given spin I, of a water molecule proton, coupled to the surroundings and with other spins are the interaction with the local paramagnetic fields and the change of the molecule dynamics due to wetting phenomena at the inner pore surface. The paramagnetic interaction is described by tensor forms that are the function of the inter-spins distance coordinates, with respect to the magnetic field, spin operator components, and the external magnetic field [1, 2]. All these interactions can be written in bilinear forms. In particular, nuclear relaxation caused by fixed paramagnetic impurities rise from the interaction between the nuclear spin and unpaired electron spins that generate a fluctuating electronic magnetic field at

Published online: 07 November 2014

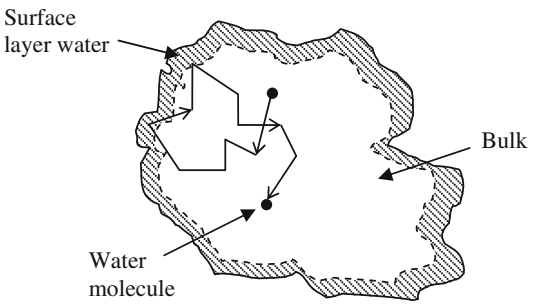

Fig. 1 Motion of a water molecule inside a pore

the resonant site. The fluctuating character of the electronic local magnetic field seen by the resonant spin I is

$$\vec{H}_{\mathrm{e}} = -\frac{1}{\gamma_I}\vec{S}(t)\cdot\hbar\overleftrightarrow{A} \tag{1}$$

For an I spin, $I = 1/2$, being in a rapid tumbling and moving water molecule in a pore, the variation of $\vec{H}_{\mathrm{e}}(t)$ is due to the electronic relaxation of $\vec{S}(t)$ rather than variations of the tensor $\hbar\overleftrightarrow{A}$. Thus, for a sufficiently low fixed external magnetic field, $\vec{H}_0$, a water molecule proton will sense an electronic spin flip each time it approaches to the pore surface. The need for a low magnetic field is because the transversal relaxation time, T_2, due to the scalar coupling is proportional to $(1 + (\omega_S - \omega_I)^2\tau_{\mathrm{e}}^2)$, where τ_{e} is the electronic correlation time, which requires the field to be weak enough in order to contribute significantly over the homonuclear dipolar coupling [1, 3]. Thus, it is convenient to have a magnetic field to be such that it generates 2 MHz proton's Larmor frequency. The picture of a water molecule, undergoing Brownian motion and rapid tumbling, inside a filled pore and sensing the surface, takes place in a crust volume surrounding the pore surface, is depicted in Fig. 1.

The most common paramagnetic atoms found in petroleum sandstone are Fe^{+3}, Mg^{+2}, and Mn^{+2}, which in small amounts as low as 1 ppm are enough to produce strong relaxation processes [1, 4].

The wetting effects at the pore surface introduce tensions on the liquid molecules, which affect the dynamic favoring semi-rotations rather than rapid tumbling as in the pore bulk. Thus, when a brine-saturated rock is immersed in a homogeneous magnetic field, the fluid protons in the pores respond to an NMR spin-echo T_2 experiment such that

$$\frac{1}{T_2} = \rho\left(\frac{S}{V}\right)_{\mathrm{pore}} \tag{2}$$

where S/V is the ratio surface to volume of the pore and the coefficient ρ is the T_2 surface relaxation strength or "relaxivity" [6].

The most convenient way to measure T_2 is by means of the Carr–Purcell–Meiboom–Gill (CPMG) [4, 7] pulse sequence, which yields the total transversal magnetization decay from which the T_2 distribution is obtained following a discrete nonlinear regularized Laplace transform [8], namely the signal amplitude $S(t; C_i, T_{2i})$ is fitted by

$$S(t; C_i, T_{2i}) = \sum_{i=1}^{n}\left\{C_i \exp\left(-\frac{t}{T_{2i}}\right) + \xi|C_{i+1} - C_i|\right\} \tag{3}$$

with the condition that $C_{n+1} = 0$ and where the coefficients C_i indicate the weight of the decay, thus providing a mean to measure the pore abundance whose sizes are characterized by T_{2i}, and ξ is the regularization coefficient of the fit.

In order to obtain a good signal to noise ratio of the NMR signal, it is required that a reasonable amount of brine must be contained in the rock pores.

2.2 The dielectric constant

The macroscopic electrical behavior of any material is described by Maxwell's equations and certain constitutive relationships. Thus, when rock is subjected to an alternated sinusoidal electric field that depends on $j\omega t$, $j = \sqrt{-1}$, being the constitutive dielectric equation and the Ohm's law

$$\begin{aligned}\vec{D} &= \varepsilon_0(1 + \chi_{\mathrm{e}})\vec{E}\\ \vec{J} &= \sigma_{\mathrm{c}}\vec{E}\end{aligned} \tag{4}$$

where $\varepsilon_0 = 8.854 \times 10^{-12}$ Fm^{-1} is the vacuum permittivity, $\chi_{\mathrm{e}} = \chi' + j\chi''$ is the complex electric susceptibility of the material, and $\vec{J}$ is the current density due to free electric charges. The Maxwell's equation for the total current density can be worked out to obtain

$$\begin{aligned}\vec{J}_{\mathrm{t}} &= \vec{J} + \frac{\partial\vec{D}}{\partial t} = j\omega\varepsilon_0\left[(1 + \chi_{\mathrm{e}}) - \frac{j\sigma_{\mathrm{c}}}{\omega\varepsilon_0}\right]\vec{E}\\ &= j\omega\varepsilon_0\left[\varepsilon_{\mathrm{r}} - \frac{j\sigma_{\mathrm{c}}}{\omega\varepsilon_0}\right]\vec{E}\end{aligned} \tag{5}$$

the quantity between brackets in (5) is a complex function of the angular frequency ω. Thus, $\vec{J}_{\mathrm{t}}$ possesses the contribution of two current densities, under the action of the applied electric field $\vec{E}$, being one due to the transport of free charges, σ_{c}, and the other term is related to oscillations of bound charge distributions, $\omega\varepsilon_0\varepsilon_{\mathrm{r}}$. Generally, experimental measurements yield only access to the total current density $\vec{J}_{\mathrm{t}}$. Therefore, it is convenient to introduce both the synthetic or complex conductivity σ^* and the synthetic or complex dielectric constant ε^*, which include both σ_{c} and $\omega\varepsilon_0\varepsilon_{\mathrm{r}}$ terms, and in so doing it renders both a generalized Ohm's law of the form

$$\vec{J}_t = \sigma^* \vec{E} \tag{6}$$

or, indifferently, a generalized constitutive dielectric equation given by

$$\vec{D}_t = \varepsilon^* \vec{E} \tag{7}$$

where $\vec{D}_t$ is the total electric displacement and ε^* is the total relative dielectric permittivity. The various quantities in Eqs. (4) and (5) are related to each other as follows

$$\begin{aligned} \sigma^* &= \sigma_c + j\omega\varepsilon_0\varepsilon_r = j\omega\varepsilon_0\left(\varepsilon_r - \frac{j\sigma_c}{\omega\varepsilon_0}\right) \\ \sigma^* &= j\omega\varepsilon_0\varepsilon^* \end{aligned} \tag{8}$$

On this ground, both complex conductivity and dielectric permittivity are perfectly equivalent, and it is possible to derive the dielectric properties of a rock from conductivity measurements, or vice versa [9, 10]. In the following, both simpler terms "conductivity" and "dielectric constant" will be used instead of "complex or synthetic conductivity" and "complex, or synthetic, relative dielectric permittivity." It is generally customary to write

$$\varepsilon^*(\omega) = \varepsilon'(\omega) - j\varepsilon''(\omega) \tag{9}$$

where ε^* is the addition of a real (ε') and an imaginary $(-\varepsilon'')$ part.

In a typical dielectric measurement, the sample is placed between the plates of a capacitor, without physical contact to them, and its measured relative dielectric constant, considering the rock containing various amounts of brine, is dependent on frequency. This often called dispersive behavior yields values of ε' and ε'' exceeding 10^4 at low frequencies, which is more than two orders of magnitude or even greater than the dielectric constant of any constituent material of the rock. At the high-frequency limit, both components attain magnitudes of the order of 10 or less and in the whole range, 10 Hz–10 GHz, and each of the components of ε^* behaves as continuous monotonic decreasing functions of the frequency. The entire behavior can be described by the overlapping contributions of four particular physical mechanisms dominating different frequency zones. These are a real constant terms, ε_∞; in the low-frequency domain, 10 Hz–10 kHz, the charge transport dominates the dielectric constant and it is described by a complex power function, $\varepsilon_{LFP}(\omega)$; in the intermediate frequency zone, 10 kHz–1 GHz, a complex function models Maxwell–Wagner, $\varepsilon_{MW}(\omega)$, polarization mechanisms; and in the high-frequency region, higher than 1 GHz, another complex power function, $\varepsilon_{HFP}(\omega)$, takes account of physical mechanisms such as molecular and collectives absorption modes [9, 10]. Thus, $\varepsilon^*(\omega)$ is written as

$$\varepsilon^*(\omega) = \varepsilon_\infty + \varepsilon_{LFPF}(\omega) + \varepsilon_{MW}(\omega) + \varepsilon_{HFLP}(\omega) \tag{10}$$

where

$$\varepsilon_{LFP}(\omega) = \frac{D}{\varepsilon_0(j\omega)^Q} \tag{11}$$

$$\varepsilon_{MW}(\omega) = \frac{\Delta\varepsilon}{1 + (j\tau\omega)^{1-\beta}} \tag{12}$$

$$\varepsilon_{HFP}(\omega) = \frac{A}{\varepsilon_0(j\omega)^N} \tag{13}$$

where $\Delta\varepsilon$, β, with $(0 < \beta < 1)$, D, A, Q and N, with $(0 < N < Q \leq 1)$ are real parameters, with $\tau \equiv \omega_{rel}^{-1}$, and $\Delta\varepsilon = (\varepsilon_s - \varepsilon_\infty)$. Additionally, by means of Eqs. (8) and (10), the conductivity can be written as

$$\sigma^*(\omega) = j\omega\varepsilon_0\varepsilon_\infty + D(j\omega)^\alpha + \frac{j\omega\varepsilon_0\Delta\varepsilon}{1 + (j\tau\omega)^{1-\beta}} + A(j\omega)^\gamma \tag{14}$$

with the exponents $\alpha = 1 - Q$ and $\gamma = 1 - N$, from where the direct current (dc) conductivity is

$$\sigma_{dc} = \frac{\sigma'(\omega)}{\omega^\alpha} = (2\pi)^\alpha \cos\left(\frac{\pi}{2}\alpha\right) D \tag{15}$$

The experimental values of σ_{dc} are obtained following a simultaneous fit of both real and imaginary components of either the conductivity or the dielectric constant [11, 12].

3 Experimental procedures, apparatus, and samples

3.1 NMR apparatus

The NMR equipment used in this work is a standard pulsed spectrometer with a working frequency in the range of 2 MHz for proton (^{1}H) resonance, and the transversal decays to obtain their characteristic times, T_2, distributions were obtained using a CPMG pulse sequence with phase alternation. The spectrometer possesses both a magnet and a sample probe adequate to hold a cylindrical rock samples with 40 mm diameter and 52 mm length.

3.2 Total and effective porosities

The total porosity, ϕ, and the effective porosity, ϕ_e, correspond to the sandstone volume occupied by the saturation brine and that which is occupied by the irreducible brine after centrifugation, respectively. Both porosities are measured gravimetrically and are used to calibrate the NMR results.

The total porosity, ϕ, is obtained from the weight of the cleaned and dried sandstone, P_0, the weight of the fully saturated sandstone, P_{SW}, and from the weight of saturated and submerged sandstone, P_{SWS}, the volume V_ϕ associated to ϕ, such that

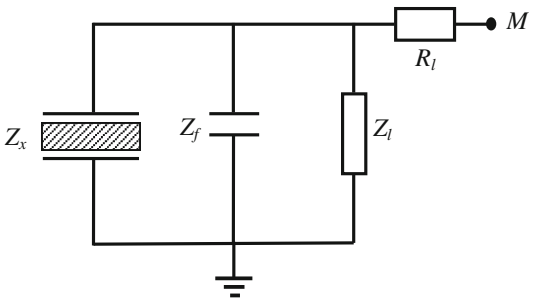

Fig. 2 Capacitive probe equivalent circuit

$$\phi = 100 \times \frac{P_{SW} - P_0}{P_{SW} - P_{SWS}} \tag{16}$$

Similarly, after obtaining the weight of the rock with its irreducible fluids, P_{SWI}, after centrifugation the effective porosity, ϕ_e is

$$\phi_e = 100 \times \frac{P_{SW} - P_{SWI}}{P_{SW} - P_{SWS}} \tag{17}$$

3.3 Dielectric measurements equipment

The apparatus used to measure the dielectric constant was an Agilent 4395A network analyzer connected to a capacitive probe. The method consists of placing the sample to be measured inside a capacitor of parallel flat circular plates and with no physical contact to the plates, which constitutes the probe circuit connected to the network analyzer at the measuring node, M, and may be schematized as depicted in Fig. 2.

The capacitor has been specially designed to maximize the signal to noise ratio, being the variable parameters both the separation between plates and the diameter which were optimized to be 4 and 40 mm, respectively. In the figure, the impedance of the capacitor without dielectric is Z_0, Z_x is the impedance of the portion of the measuring capacitor occupied by the dielectric material, and Z_f is the impedance associated to the fringe electric field lines of the measuring capacitor and the portion of the capacitor unoccupied by the sample; finally, Z_l and R_l are the line reactive impedance and its ohmic resistance, respectively. Importantly, the parallel capacitive impedances Z_x, Z_l, and Z_f must be determined experimentally. Additionally, in order to properly measure the dielectric constant, it is necessary to know the limits and behavior with frequency of the capacitive probe. This is achieved by determining the high-frequency limit at which the probe starts to show a departure from its capacitive behavior, above 200 MHz, which strongly depends of the material of the plates and. The low-frequency limit is fixed by the network analyzer sensitivity, 5 Hz. Thus, the complex dielectric constants of three samples were obtained in the frequency range of 100 Hz–200 MHz by measuring the real and imaginary components of the electric admittance, namely the conductance and the susceptance of the capacitive probe with the sample as a dielectric, within the experimental errors of the measurements of ±0.2 μS. Therefore, having a dielectric filling completely the space between the plates, with an area A and a separation d, and disregarding the fringe field contribution the complex conductivity $\sigma^*(\omega)$ is related to the complex admittance Y by

$$\sigma^* = Y\frac{d}{A} = \frac{Y}{\lambda_0} = j\omega\varepsilon_0\varepsilon^* \tag{18}$$

Since it is cumbersome to obtain a rock sample to fill completely the inter-plate volume and to cancel the contribution of the fringe field to the capacitance determination, the procedure consists to measure separately both the total admittance of the capacitor without the sample, Y_c, and the admittance with the sample, Y_s, such that

$$\begin{aligned} Y_c &= Y_L + Y_f + Y_0 \\ Y_s &= Y_L + Y_f + Y_x \end{aligned} \tag{19}$$

where Y_x and Y_0 are the admittances of the portion of the capacitor with the sample and that of the same portion without the sample. The extra capacity is included in Y_f. Subtracting both admittances of (17) and taking into account the result of (16), it follows

$$Y_x - Y_0 = \varepsilon_0\omega\lambda_0[\varepsilon'' + j(\varepsilon' - \varepsilon_0)] \tag{20}$$

From the admittance definition,

$$Y_x - Y_0 = G_x - G_0 + j(B_x - B_0) \tag{21}$$

Thus, combining (20) and (21) and taking into account that for sedimentary rocks $\varepsilon' \gg \varepsilon_0$ for frequencies such that $\nu \leq 200$ MHz, it follows

$$\begin{aligned} \Delta G &= \varepsilon_0\omega\lambda_0\varepsilon'' = \lambda_0\sigma'(\omega) \\ \Delta B &= \varepsilon_0\omega\lambda_0\varepsilon' = \lambda_0\sigma''(\omega) \end{aligned} \tag{22}$$

3.4 The centrifuge

The centrifuge used for this work is a standard one capable to hold plugs with the previously set forth dimensions and whose rotating arm length is $r_{ext} = 0.217$ m at the farthest end of the plug. The centrifuge is able to reach a maximum rotation speed of about 5,000 rpm and also possesses a high-impact glass cover such as to allow the measurement of the evacuated fluids volume collected in transparent calibrated glass tubes of the sample holders, with the use of a stroboscopic light.

Considering a fluid constrained to the inside of a capillary tube, it exhibits a capillary pressure, p_c, given by

$$p_c = \frac{4\vartheta\cos\theta}{\varphi_c} \tag{23}$$

where ϑ is the surface tension, which depends on the fluids, for water $\vartheta = 7 \times 10^{-2}$ N/m, may be assumed, $\theta \leq 20°$ is the contact angle at the solid liquid interface, and φ_c the capillary diameter. When the centrifuge rotates at an appropriate frequency ω, there is a radius r, it being a point in the plug, at which the capillary pressure equals the excerpted pressure due be the fluid (brine). Therefore, the fluid between r and r_{ext} exerts a pressure at the point r_{ext} of the plug given by

$$p(r_{ext}) = \rho\omega^2 r\left(r_{ext} - \frac{r}{2}\right) - p_c, \quad 0 \leq r \leq d = r_{ext} - r_{int} \tag{24}$$

where ρ is the brine density and d the length of the plug. Thus, at the minimum frequency for which the whole brine of the plug contributes to the pressure $p(r_{ext})$ holds

$$\frac{1}{2}\rho\omega^2 d^2 = \frac{4\vartheta\cos\theta}{\varphi_c} \tag{25}$$

The next step is to set the frequency such that the pressure at r_{ext} is 10 psi $\cong$ 68.95 kPa for a water column of height d, the standard value to evaluate porosity and permeability of petroleum rocks [4, 5]. Additionally, in order to obtain a sedimentary rock with the irreducible fluids homogeneously distributed, the centrifugation is performed along two opposite directions until constant weight is achieved.

3.5 The samples

The studied rocks were three, two commercially acquired bereas from Berea Sandstone Petroleum Cores, B1 and B2, sample code K of relatively high porosity and permeability, and the third a shaly rock with kerogen forming part of the cement of the sand grains having both low porosity and permeability, obtained from oil geological formations from one prospect oil well of the Neuquén basin in Argentina. The bereas chemical composition is the following: silica (SiO_2) 93.13 %, alumina (Al_2O_2) 3.86 %, ferric oxide (Fe_2O_3) 0.11 %, ferrous oxide (FeO) 0.54 %, magnesium oxide (MgO) 0.25 %, calcium oxide (CaO) 0.10 %.

The shale rock is formed by stratigraphic sand conglomerates dominated by volcanic fragments with a predominance of feldspathic litharenites, $\sim$58 %. This framework composition records erosion of Triassic–Jurassic volcaniclastic rocks, which was exhumed as a result of Late Jurassic inversion. The shale is characterized by a moderate content of mafic (silicate) volcanic rock sands and plagioclase (family of tectosilicate minerals within the feldspar). The clay and kerogen assemblage is interpreted as the result of a complex set of factors, including source rock, climate, transport, and diagenesis. Post-depositional processes produced significant variations in the original

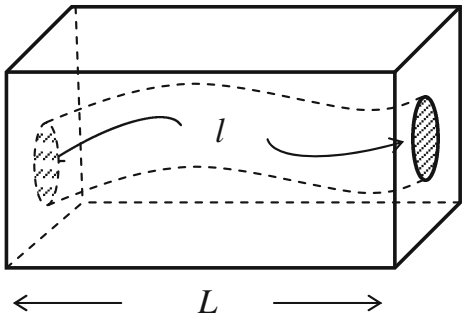

Fig. 3 Pore channel with tortuosity

compositions, especially the fine-grained deposits. The sediments are characterized by moderate SiO_2, $\sim$19 %, contents with variable and less abundances of K_2O and Na_2O, and a relatively high proportion of ferromagnesian paramagnetic elements [13].

Additionally, all samples were packed with a thin Teflon film such that to avoid water evaporation and to introduce little perturbation to NMR and DC measurements.

Sandstone cleaning and saturation is a process that involves cleaning the rocks in a soxhlet with a solvent solution of ethanol (20 %) and toluene (80 %), while the shale is cleaned only with toluene. This process is followed by drying the rock in an oven at temperatures around $T \leq 70$ °C in order to evaporate any solvent remnant. Thus, the total porosity is obtained by weight difference between the saturated and dried sample. To determine the total proton content of the shale, the weight difference is taken for both a powdered bit of the sample and that corresponding to the sample cleaned with the solvents and dried, since centrifugation does not remove all the fluids.

3.6 Petrophysical applications

The aim of all previous developments is to identify the "Tortuosity" index of a porous system by means of Archie's law [14]. Strictly speaking, Archie's law relates the formation factor F_R, which is given by the ratio between the dc electric resistivity of both the saturated rock, ρ_R, and that of the brine or saturation solution, ρ_{ss}, to the average tortuosity index, T, the porosity, ϕ, and the saturation factor, S_{ss}, of the sedimentary rock as

$$F_R = \frac{\rho_R}{\rho_{ss}} = \frac{T}{\phi^m S_w^n} \tag{26}$$

where m is the cementation exponent or calcareous concentration, $1.8 \leq m \leq 2.15$, and n the saturation exponent, respectively. For cleaned and fully hydrated sandstones, $S_w = 1$, and for the majority of rocks, m and n have approximately the same range and are usually assumed as $m \cong n \cong 2$. The tortuosity index T and is defined as the

Table 1 where $\sigma_{ss} = 12.6\ \mathrm{Sm}^{-1}$, and NB stand for no bugs

Sample	$\tau\ (10^{-6}\mathrm{s})$	$\sigma_{dc}\ (\mathrm{Sm}^{-1})$	D	$\Delta\varepsilon$	ε_∞	α	β	$\phi\ (\%)$	T	$T_{2\mathrm{cutoff}}$ (ms)
Saturated berea B1	19×10^{-3}	1.13×10^{-1}	9.4×10^{-2}	207	16.1	0.101	0.21	22.8	5.8	–
Centrifuged berea B1	2.02×10^{-3}	1.01×10^{-5}	8.8×10^{-6}	205	15.2	0.082	0.22	3.9	1,996	62.8
Dried berea B1	7.3×10^{-4}	7.72×10^{-7}	6.5×10^{-7}	50	7.5	0.019	0.28	NB	–	–
Saturated berea B2	28×10^{-3}	9.6×10^{-2}	8.24×10^{-2}	161	14.2	0.088	0.47	22.2	6.3	–
Centrifuged berea B2	4.64×10^{-3}	8.34×10^{-6}	7.25×10^{-6}	160	14	0.085	0.44	3.8	2,182	61.2
Dried berea B2	9.02×10^{-4}	9.2×10^{-7}	8.6×10^{-7}	50	8	0.031	0.44	NB	–	–
Saturated shale	0.24	2.79×10^{-6}	3.21×10^{-6}	88.4	7.1	0.09	0.42	8.2	30×10^3	–
Centrifuged shale	0.24	1.06×10^{-6}	9.01×10^{-7}	75	5.3	0.09	0.42	7.2	62×10^3	34
	108			44						

ratio between the length l of the average capillary channel, connecting the two surfaces of the rock, with length L, of the sample Fig. 3. For shaly rocks with very low permeability, it is convenient to replace in (26) the product $\phi^m S_w^n$ by an apparent porosity, ϕ_a^m, since the determination of the saturation factor requires of elaborated laboratory tests [14].

In order to determine T, it is necessary to measure both ρ_{ss} and ρ_R that bring about important experimental drawbacks, since due to the roughness and irregularity of the rock surface it is very difficult to get a proper contact with electrodes to measure the resistivity; moreover, since the water distribution on the surface is quite heterogeneous by means of a simple electrical contact, it ends up measuring the surface resistivity. Therefore, the best method is to measure the conductivity for an alternated field through the displacement current, and to extrapolate its value at zero frequency, and from this value to obtain the resistivity.

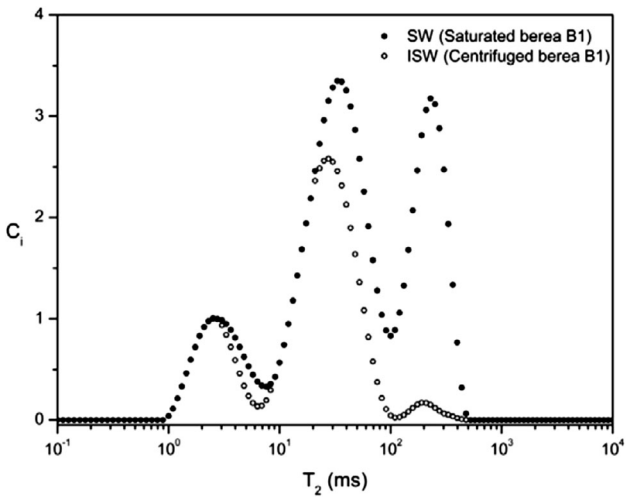

Fig. 4 Pore size distribution, C_i versus T_2, corresponding to both saturated and centrifuged berea B1

4 Experimental results

Following both NMR and dielectric measurements, the processed results are summarized in Table 1. But previously, as an example, to depict the experimental measured data, the following figures show the corresponding ones of the berea sandstones B1 and the shale.

Figures 4 and 5 depict the pore size distribution, SW and ISW (saturation water and irreducible saturation water), and the normalized incremental porosity of berea B1, and they also show the values of $T_{2\mathrm{cutoff}}$ and the Bulk Volume Movable fluid (BVM) [4].

Figures 6 and 7 show the pore size distribution corresponding to the saturated and centrifuged shale, and Fig. 8 shows its normalized incremental porosity.

Figures 9, 10, and 11 show the components of the dielectric constant measurements corresponding to the

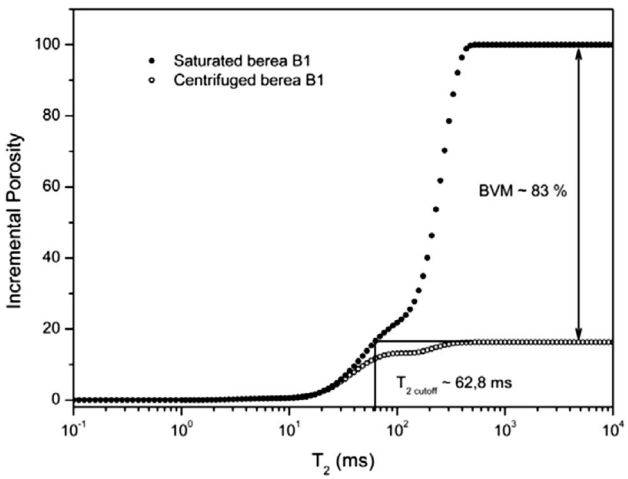

Fig. 5 Normalized incremental porosity versus T_2 corresponding to both saturated and centrifuged berea B1

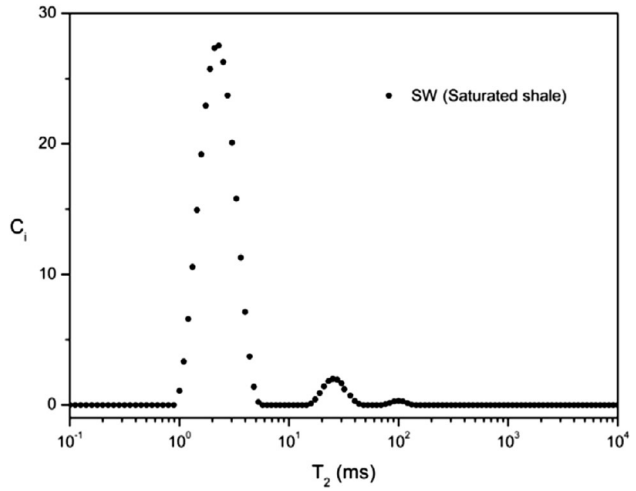

Fig. 6 Pore size distribution, C_i versus T_2, of the saturated shale

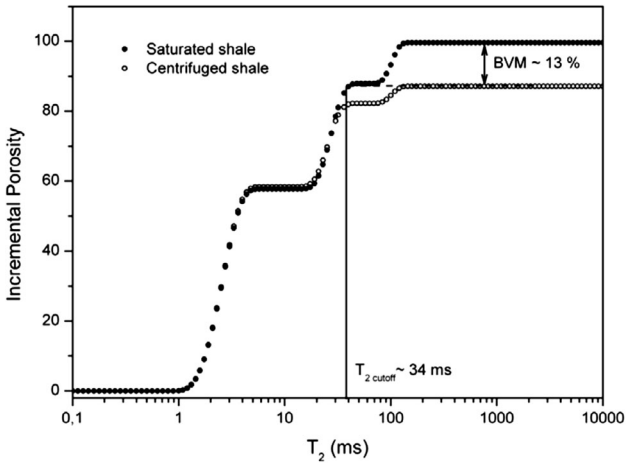

Fig. 8 Normalized incremental porosity versus T_2 corresponding to both saturated and centrifuged shale

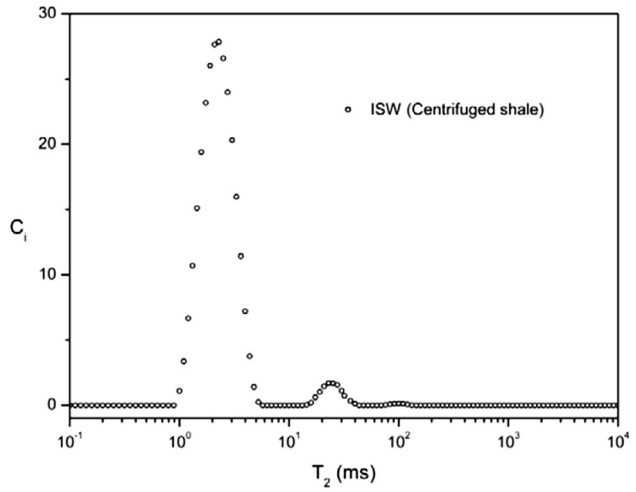

Fig. 7 Irreducible pore size distribution, C_i versus T_2, of the centrifuged shale

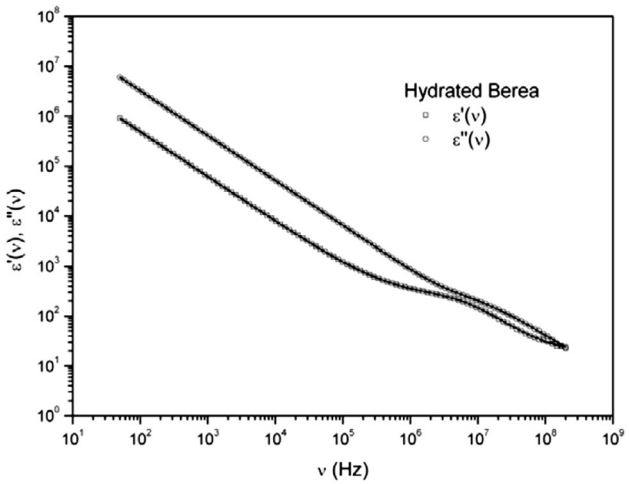

Fig. 9 Dielectric constant vs frequency of fully saturated berea B1, $\sigma_{sd} = 2$

saturated, centrifuged, and dried berea B1, respectively. Additionally, the continuous line depicts the data fit and in the figure caption the standard deviations $\sigma_{sd} = \sqrt{N^{-1}\sum_i \left(x_i - x_{t,i}\right)^2}$ ($x_{t,i}$ is the fitted value) are included.

Figures 12 and 13 show the components of the dielectric constant measurements corresponding to the saturated and centrifuged shale, respectively, and Fig. 14 shows the imaginary part of Maxwell–Wagner term of the DC.

5 Conclusions

The experimental results show that the particular experimental method proposed is excellent for measuring dielectric constant, obtaining from this and gravimetric measurements of the porosity the tortuosity index associated to the pore system of a particular sedimentary rock, having previously determined the measuring frequency ranges of the capacitive probe.

Results related to the petrophysics of porous sedimentary rock are shown in Table 1. The systems studied were two K berea sandstones, having relatively good porosity and permeability, and a sedimentary shaly rock of low porosity and poor permeability.

In particular, both bereas show a regular behavior, for which the conductivity decreases as brine is centrifuged. Additionally, it is not observed changes in the wettability of pores walls with the decrease in the amount of water in the rock. This is reflected in the variation of the polarization relaxation times decreases with the size of hydrated pores corresponding to saturated and centrifuged sample,

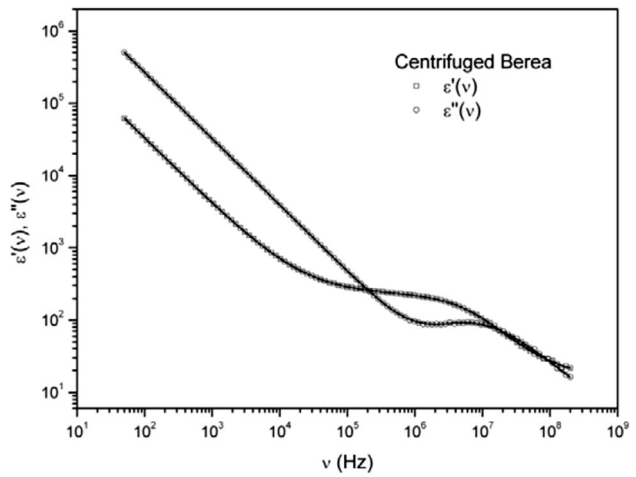

Fig. 10 Dielectric constant vs frequency of centrifuged berea B1, $\sigma_{sd} = 2.8$

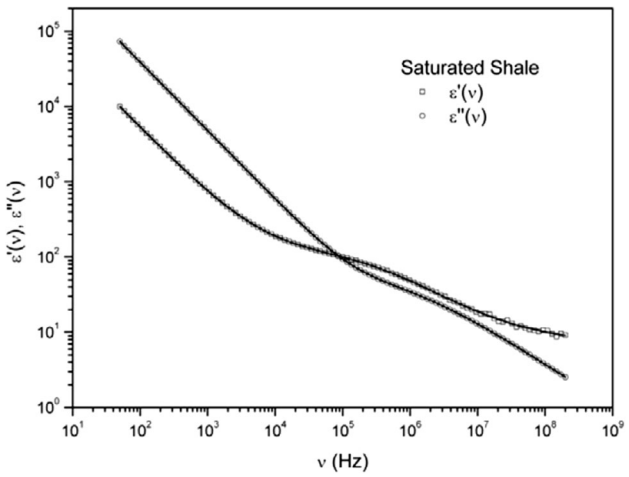

Fig. 12 Dielectric constant vs frequency of saturated shale, $\sigma_{sd} = 5.1$

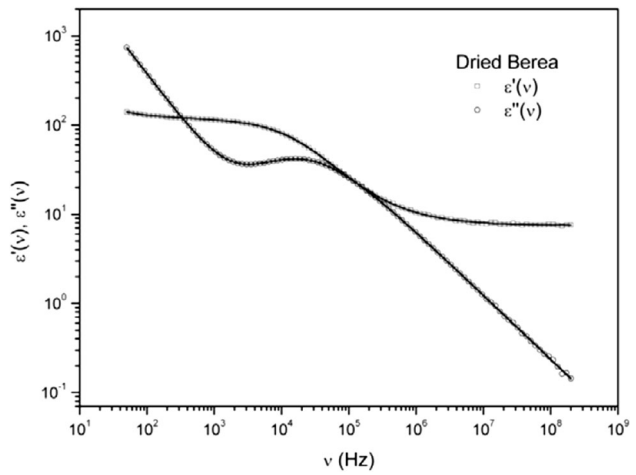

Fig. 11 Dielectric constant vs frequency of dried berea B1, $\sigma_{sd} = 3.8$

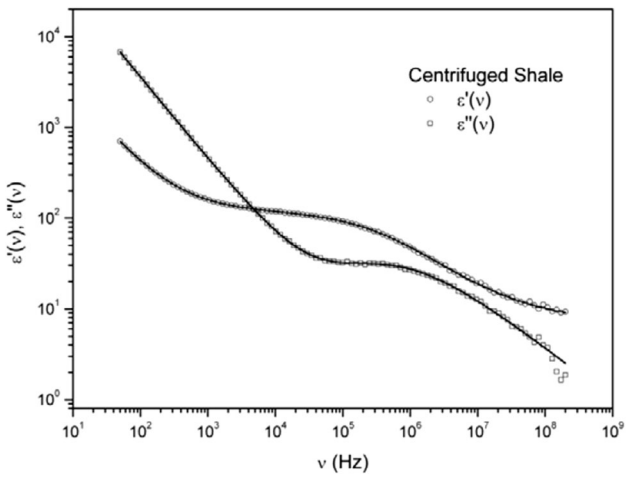

Fig. 13 Dielectric constant vs frequency of centrifuged shale, $\sigma_{sd} = 6.2$

and the MW DCC term is characterized by a single relaxation time. The centrifugation followed by the drying process leave the bereas without hydrated irreducible bugs (closed pores with water), namely no proton NMR signal is detected after this process.

In the fully saturated shale, the situation is similar to the bereas, but after subjected to centrifugation, the data show the occurrence of a second type of surface wettability in the pores, which is reflected by the appearance of a second MW mechanism of polarization in the imaginary component of the DCC [15], Fig. 14. This is due to the fact that for low water saturation, the shape and not the size of water inclusions plays the most important role, determining the features of electric response. Hence, more elongated is the polarized charge distributions that yield higher polarization strengths and slower relaxation times charge of MW DCC term [16].

In addition, we understand that a significant improvement in theoretical model of wettability effects will deepen the studies of variations of the relaxation time for different surface porous systems with different known feature types.

Taking into account that the centrifugation pressure gradient is 5 psi/inch $\cong$ 13.79 kPa/cm and from (23), where an average $\theta \approx 20°$ was assumed, and considering that for a cylindrical tube with length $l = TL$, its pore size is given by the ratio

$$a = \frac{V}{S} = \frac{l\varphi_c}{\varphi_c + 4l} \cong \frac{\varphi_c}{4}, \quad l \gg \varphi_c \tag{27}$$

that allows the determination of the maximum pore channel section φ_c that traps the irreducible fluids. These results may be correlated to the corresponding $T_{2cutoff}$ values for each sample and from (2) obtaining the relaxivity factor

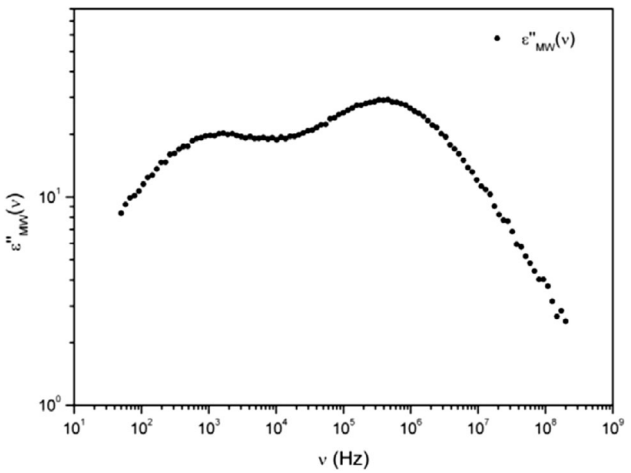

Fig. 14 Imaginary part of Maxwell–Wagner term versus frequency of centrifuged shale

$$\begin{aligned} \rho(\mathrm{B1}) &= 38.53\ \mu\mathrm{ms}^{-1} \\ \rho(\mathrm{B2}) &= 39.54\ \mu\mathrm{ms}^{-1} \\ \rho(\mathrm{shale}) &= 75.62\ \mu\mathrm{ms}^{-1} \end{aligned} \tag{28}$$

Having achieved the relaxivity factor an approximate metric scale to the T_2 axis of the pore distribution, Figs. 4, 5, 6, 7, and 8 are shown. Notice that an absolute quantitative metric assignation is not possible considering that the model assumes the rock constituted by a system of parallel tortuous pore channels. Nevertheless, with a good degree of approximation, these results are relevant to well loggers.

Acknowledgments We thank to Dr. R. Astini from the Geology Department of the Facultad de Ciencias Exactas Físicas y Naturales for his help in sample preparation. This research has been supported Secyt-Universidad Nacional de Córdoba.

References

1. A. Abragam, *The Principles of Nuclear Magnetism* (Oxford University Press, New York, 1961)
2. M. Mehring, *Principles of High Resolution NMR in Solids* (Springer, Berlin, 1983)
3. M.A. Chesta, M.E. Ramia, S. Jeandrevin, C.A. Martín, Appl. Phys. A **97**, 301–307 (2009)
4. R.G. Coates, L. Xiao, M.G. Prammer, *NMR Logging, Principles and Applications* (Halliburton Energy Services, Houston, 1999)
5. C.A. Martín, M.E. Ramia, L. Barberis. J. Soc. Pet. Eng. SPE-107781-PP (2007)
6. R.L. Kleinberg, W.E. Kenyon, P.P. Mitra, J. Magn. Reson. A **108**(2), 206 (1994)
7. C.P. Slichter, *Principles of Magnetic Resonance* (Springer, Berlin, 1990)
8. A.M. Niell, C.A. Martín, M.E. Ramia, Ann. Magn. Reson. **7**, 1–44 (2008)
9. N. Bona, E. Rossi, S. Capaccioli, Soc. Pet. Eng. **69741**, 80 (2000)
10. K.S. Cole, R.H. Cole, J. Chem. Phys. **9**, 341–351 (1941)
11. M.E. Ramia, C.A. Martín y M.A. Chesta, Trabajos de Física, UNC—FAMAF, No 14, www.famaf.unc.edu.ar, (2012)
12. C.A. Martín, G.A. Monti, J. Comput. Phys. **75**, 244 (1998)
13. L.A. Spaletti, I. Queralt, S.D. Matheos, F. Colombo, J. Maggi, J. South Am. Earth Sci. **25**(4), 440 (2008)
14. T. Djebar, E.C. Donaldson, *Petrophysics* (Elsevier, Amsterdam, 2004)
15. P.C. Lysne, Geophysics **48**, 775 (1983)
16. N. Bona, E. Rossi, S. Capaccioli, Proc. Soc. Core Anal. **9925**, 1 (1999)